

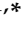





## Article

# A Compact Weighing Lysimeter to Estimate the Water Infiltration Rate in Agricultural Soils

Laura Ávila-Dávila <sup>1,2</sup>, Manuel Soler-Méndez <sup>2</sup>, Carlos Francisco Bautista-Capetillo <sup>1</sup>, Julián González-Trinidad <sup>1,\*</sup>, Hugo Enrique Júnez-Ferreira <sup>1</sup>, Cruz Octavio Robles Roveló <sup>1</sup>  
and José Miguel Molina-Martínez <sup>2,\*</sup>

<sup>1</sup> Research Group Doctorado en Ciencias de la Ingeniería, Autonomous University of Zacatecas, Campus UAZ Siglo XXI, Zacatecas 98160, Mexico; laura\_14avila@uaz.edu.mx (L.Á.-D.); baucap@uaz.edu.mx (C.F.B.-C.); hejunez@uaz.edu.mx (H.E.J.-F.); corr03@hotmail.com (C.O.R.R.)

<sup>2</sup> Research Group Ingeniería Agromófica y del Mar, Technical University of Cartagena, Campus Alfonso XIII, ETSIA, 30203 Cartagena, Spain; manuel.ia@agrosolmen.es

\* Correspondence: jgonza@uaz.edu.mx (J.G.-T.); josem.molina@upct.es (J.M.M.-M.);  
Tel.: +34-968-32-5929 (J.M.M.-M.)

**Abstract:** Infiltration estimation is made by tests such as concentric cylinders, which are prone to errors, such as the lateral movement under the ring. Several possibilities have been developed over the last decades to compensate these errors, which are based on physical, electronic, and mathematical principles. In this research, two approaches are proposed to measure the water infiltration rate in a silty loam soil by means of the mass values of a lysimeter weighing under rainfall conditions and different moisture contents. Based on the fact that with the lysimeter it is possible to determine acting soil flows very precisely, then with the help of mass conservation and assuming a downward vertical movement, 12 rain events were analyzed. In addition, it was possible to monitor the behavior of soil moisture and to establish the content at field capacity from the values of the weighing lysimeter, from which both approach are based. The infiltration rate of these events showed a variable rate at the beginning of the rainfall until reaching a maximum, to descend to a stable or basic rate. This basic infiltration rate was  $1.49 \pm 0.36$  mm/h, and this is because soils with fine textures have reported low infiltration capacity. Four empirical or semi-empirical models of infiltration were calibrated with the values obtained with our approaches, showing a better fit with the Horton's model.

**Keywords:** soil moisture; water balance; vertical movement; drainage; rainfall; water mass



**Citation:** Ávila-Dávila, L.; Soler-Méndez, M.; Bautista-Capetillo, C.F.; González-Trinidad, J.; Júnez-Ferreira, H.E.; Robles Roveló, C.O.; Molina-Martínez, J.M. A Compact Weighing Lysimeter to Estimate the Water Infiltration Rate in Agricultural Soils. *Agronomy* **2021**, *11*, 180. <https://doi.org/10.3390/agronomy11010180>

Received: 27 November 2020

Accepted: 14 January 2021

Published: 18 January 2021

**Publisher's Note:** MDPI stays neutral with regard to jurisdictional claims in published maps and institutional affiliations.



**Copyright:** © 2021 by the authors. Licensee MDPI, Basel, Switzerland. This article is an open access article distributed under the terms and conditions of the Creative Commons Attribution (CC BY) license (<https://creativecommons.org/licenses/by/4.0/>).

## 1. Introduction

To understand the behavior of the hydrological cycle in the soil remains a challenge for science, specifically the movement of water through the soil and its capacity to retain it. To estimate the water exchange between a well-defined portion of soil and other physical systems to which water is transferred through evaporation, transpiration, percolation or drainage, several methods as gravimetric, tensiometry, humidity sensing, and lysimetry have been proposed in the specialized literature [1–3].

Infiltration is the hydrological process that describes the entry of water into a soil, and the amount of water that enters the soil in a given time represents the infiltration rate [4,5]. It is variable in space and time, due to hydrodynamic and physical soil properties, flow conditions, and cultivation practices, among others [6–9]. As water enters the soil profile through the forces of adhesion, the interaction of water and soil particles, and gravity, it fills the pores of the soil, defining a wet front as it passes through the soil profile. If the soil has a good structure and large pores, its infiltration rate will be high (as in the case of coarse-textured soils) and it will reach a deeper wet front compared to a fine-textured soil whose pores are smaller. It is assumed that if the soil is at its lower limit of initial

moisture content, a higher infiltration rate would be observed [10–14]. This is not true for hydrophobic or water-repellent soils caused by high organic matter and clay content [15].

The first model to describe the movement of water into a saturated soil profile is the well-known Darcy's law, which states that the flow through the soil column is linearly proportional to the cross-section and the hydraulic gradient [4]. Years later, a correction was made to apply it to unsaturated soils with the Darcy–Buckingham's law, which states that if the liquid pressure increases, the proportionality constant will increase, because the air-filled spaces will decrease [7]. Richards [16] proposed another model for unsaturated soil as a result of Darcy's law and the concept of the capillary potential of liquids in a porous media. There are simplified models based on soil physical properties were developed for unidirectional infiltration. One of them is the well-known Kostiakov's model developed from experimental observations related to water volume moving on soil versus time, but it has no physical meaning with the soil [4]. Similarly, experimental techniques—such Horton's model—have been proposed which arise from simplifications made to continuity equation to estimate infiltration rate [17].

The single and double ring infiltrometers allow to measure the soil infiltration rate in field tests, due to their simplicity and easy operation in one dimension [6,18,19]. These instruments assume that the infiltration is vertical, and although they are easy to use, the test requires sufficient time to obtain a better estimation of the infiltration [20,21]. Such assumption it is not true in most cases, then a better understanding of this phenomenon occurs when more precise instruments are used to measure the infiltration rate taking into account the water movement in other directions, one of which is the weighing lysimeter, which is based on water balance flows. This allows for the estimation of water and solute flows in the entire profile of saturated or unsaturated soils [22–24].

The weighing lysimeter can be used in experiments under different conditions (crop variety, ground composition, atmospheric conditions, and irrigation events) and to extrapolate the behavior to great land extensions and optimize the hydric resources [25,26]. These devices have been used to quantify precipitation, condensation, and determine crop evapotranspiration [27–33]. Moreover, they could be used to characterize the contribution of groundwater and determine the percentage of leachate for a crop in real-time [34] or the upward water flow of a groundwater table [35]. Studies of water movement into the soil with the use of the lysimeter and different sensors of water content or matric potential were conducted [36–38]. To better understand the behavior of infiltration and surface runoff when there is heavy rain, it is necessary to further investigate the lysimeters calibration. See Haselow et al. [27] for information to understand this phenomenon.

Usually, lysimeters have been used for research purposes at experimental facilities of agricultural centers sponsored by governments. Although over time, the dimensions of weighing lysimeter have been declining, they are still of robust architecture and relatively expensive, especially thinking of furthering their use among farmers. The main objective of this work was to determine the infiltration rate of a silty loam soil in function of the soil field capacity content, using the mass data of a compact weighing lysimeter. The results were used to calibrate the Kostiakov's models, the modified Kostiakov's model, the Horton and the Philip models by using the data collected with the lysimeter.

## 2. Materials and Methods

### 2.1. Study Area

Field measurements were performed on Las Tiesas farm with one hectare of extension in Albacete, Spain (39°3'31" N, 2°6'04" W) at an elevation of 695 m.a.s.l. (Figure 1) during 2017. Albacete is characterized by a semi-arid climate, with an average annual rainfall of 384 mm and high temperatures in summer (average maximum value of 40 °C, minimum of −6 °C, and an average of 30 °C).

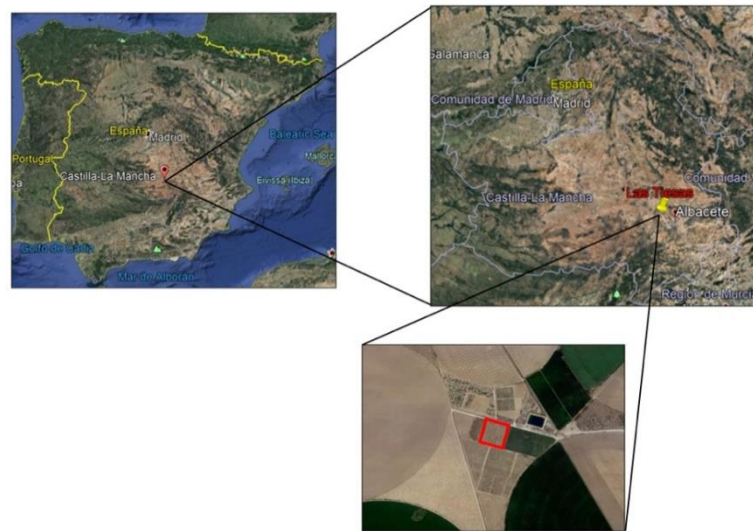


**Figure 1.** Location of the Study Area [39].

The soil texture was classified as silt loam, based on the soil percentages obtained with Bouyoucos hydrometer method and the USDA texture triangle figure [40]. Percentages of soil granulometry are 27.1% sand, 51.5% silt, and 21.4% clay; an organic matter of 2.77%, and a bulk density of  $1.38 \text{ g/cm}^3$ . The hydrodynamic characteristics of the field capacity and permanent wilting point were obtained by the membrane and pressure plate apparatus, which resulted in  $0.35 \text{ cm}^3/\text{cm}^3$  and  $0.16 \text{ cm}^3/\text{cm}^3$ , respectively. The initial soil moisture content on February 8 were the experiment started was inferred knowing the bulk density and total volume with  $0.23 \text{ cm}^3/\text{cm}^3$ .

## 2.2. Materials

The compact weighing lysimeter,  $L_{TSI}TN-AC-E_1$  model (teleNatura, Alicante, Spain), consists of two vessels. The upper vessel called soil vessel has dimensions of  $0.56 \text{ m} \times 0.96 \text{ m}$  and  $0.35 \text{ m}$  depth in the center, which stores a volume of the reconstituted soil from the plot trying to keep the same conditions from where it is extracted, with a resolution of  $20 \text{ g}$  or  $0.033 \text{ mm}$  (Figure 2). The soil is isolated of its environment in such a manner that the lateral and capillary rise underground flows are zero [26], so that the water balance terms can be accurately obtained.

The second vessel is located below the previous one. It is called drainage vessel and serves to store the excess of water drained by the soil profile with a resolution of  $1 \text{ g}$  (or  $0.002 \text{ mm}$ ). The soil vessel has a hole in the lower central part that allows the water flows to an electrovalve, then goes to a funnel and finally reaches the drainage vessel, where it will be stored and weighed (Figure 2c). The drainage vessel was configured to store only  $3000 \text{ g}$  of water, so when this increase is reported, the electrovalve located under it is activated and starts emptying it, while this occurs the electrovalve of the soil vessel is closed to avoid losses of water quantification. Once the emptying process has been completed, the electrovalves return to their initial state, opening the soil vessel one and closing the drainage vessel one, allowing the water flow from the soil vessel to the drainage vessel.

The mass variations of both vessels are detected by load cells, four for the soil vessel and one for the drainage vessel. These load cells send an electrical signal to the datalogger (CR300 model, Campbell Scientific, Logan, UT, USA), according to the deformation suffered by the object that they are supporting. This electrical signal is converted to a mass value by the same datalogger. According to the Spanish norm UNE 500520 [41], the mass data of the two vessels was sampled every second and the average value of  $60 \text{ s}$  (one minute) was registered as an instantaneous value. This guarantees the maximum quality and representativeness of the data obtained. For further details of the compact weighing lysimeter see the work of Nicolás-Cuevas et al. [42].

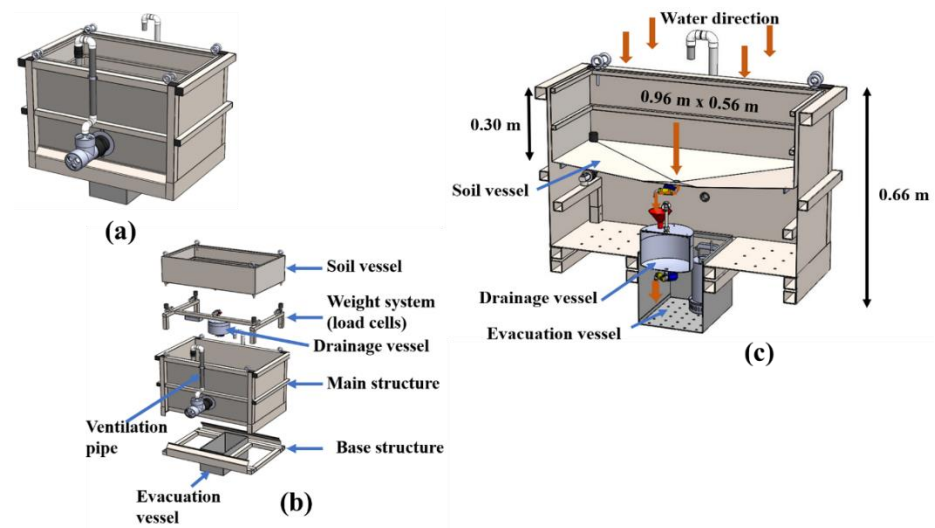


**Figure 2.** Compact weighing lysimeter (a) full view, (b) exploded view and (c) water movement through the vessels.

### 2.3. Flow Calculation

The lysimeter contains an isolated soil profile, so that is possible to determine the water inputs and outputs in the soil based on the mass data records, through the mass balance equation, shown in Equation (1):

$$\frac{dS}{dt} = \frac{dP}{dt} + \frac{dIR}{dt} - \frac{dD}{dt} - \frac{dET}{dt} - \frac{dSr}{dt} \quad (1)$$

where  $\pm \frac{dS}{dt}$  is the change of soil water storage (g),  $\frac{dP}{dt}$  is the amount of water by precipitation (g),  $\frac{dIR}{dt}$  is the amount of water by irrigation (g),  $\frac{dD}{dt}$  is the amount of water drainage beyond the root zone (g),  $\frac{dET}{dt}$  is the amount of water by the crop evapotranspiration (g), and  $\frac{dSr}{dt}$  is the surface runoff (g) along interval of time [6].

In this work, only the rainfall events were analyzed to know the rate of entry of water into the soil. The rainfall has a longer duration of application and therefore gives a better accuracy of the results. So, variables as irrigation and evapotranspiration were not considered, except in determining  $\theta_{FC}$ , because they cannot occur when there is rain [32,43], so we reformulate Equation (1) as Equation (2):

$$\frac{dS}{dt} = \frac{dP}{dt} - \frac{dD}{dt} - \frac{dSr}{dt} \quad (2)$$

Surface runoff is neglected because it was not observed here. The only known variables are the accumulated masses of the soil vessel ( $S$ ) and the drainage vessel ( $D$ ), so the flow is determined by the increase in the mass ( $m$ ) of the vessel over time [32], as the Equation (3):

$$\frac{dS}{dt} \text{ or } \frac{dD}{dt} = \frac{m_{t_{i+1}} - m_{t_i}}{t_{i+1} - t_i} \quad (3)$$

where  $\frac{dD}{dt}$  is the flow of drainage vessel over time,  $\frac{dS}{dt}$  is the flow of the soil vessel over time,  $t_i$  is the time in the instant  $i$  and  $t_{i+1}$  is the time in the instant  $i + 1$ .

Rainfall is calculated based on literature reports [27,32,43,44], so that the lysimeter must satisfy the condition  $\frac{dD}{dt} + \frac{dS}{dt} > 0$ . Therefore, the following Equation (4) was used:

$$\frac{dP}{dt} = \frac{dD}{dt} + \frac{dS}{dt} \quad (4)$$

#### 2.4. Calculation of the Infiltration Rate of Water into the Soil

The water infiltration has a downward vertical behavior in the lysimeter [26], and conditions of free drainage [7]. When the soil moisture was below field capacity water content, the increments of soil water stored in the soil vessel represent the soil infiltration rate  $\frac{dI}{dt}$  without any drainage component  $\frac{dD}{dt}$ . The infiltration rate was then represented with the following Equation (5) which was called Approach 1 [45]:

$$\frac{dI}{dt} = \frac{dS}{dt} \quad (5)$$

However, once the soil reached the water content at field capacity, it is no longer able to store more water and thus, the incoming water will be drained [45]. In that way, the sum of soil water storage and drainage represents the water infiltration rate of the soil profile. The infiltration rate model is represented as the Equation (6) which was called Approach 2:

$$\frac{dI}{dt} = \frac{dS}{dt} + \frac{dD}{dt} \quad (6)$$

Both approaches are valid if the water content at soil saturation is not reached due to the rainfall rate not overpassing the soil basic infiltration capacity. In this experiment the soil never overpass the saturation capacity, therefore there was no surface runoff. This complies with the principle of mass conservation and continuity equation.

The resulting flows and infiltration rate are representing the area of the lysimeter ( $0.54 \text{ m}^2$ ), so with the assumption that 1 L of water is equal to 1 kg of water mass and that 1 mm is equal to  $1 \text{ L/m}^2$  [27], 1 kg/min of lysimeter is equal to 1.85 kg/min or 1.85 mm/min of  $1 \text{ m}^2$  of surface.

The irrigation events were not analyzed because their time and volume of application were small, so they do not allow a visualization of the infiltration capacity curve. The infiltration rate was constant throughout the two or three hours that the irrigations lasted.

#### 2.5. Estimation of Soil Moisture Content

The soil profile water content inside the soil vessel was determined by the gravimetric method, since the mass of the wet soil profile was known at any time. Once obtained, the gravimetric water content was converted to volumetric ( $\theta_v$ ) as in Equation (7):

$$\theta_v = \left( \frac{m_i - m_{dry}}{m_{dry}} \right) \times \rho_b \quad (7)$$

where  $\theta_v$  is the volumetric water content is of the soil at instant  $i$  ( $\text{m}^3/\text{m}^3$ ),  $\rho_b$  is the bulk density of the soil,  $m_i$  is the wet mass of the soil inside the soil vessel at instant  $i$  (g or kg) and  $m_{dry}$  is the dry mass of the soil inside the soil vessel. This last value was determined from the apparent density of the soil and the total volume of the soil vessel ( $0.161 \text{ m}^3$ ) [13]. The moisture content at field capacity ( $\theta_{FC}$ ) was established two or three days after the rain events, when the soil stopped draining and the soil vessel value was constant, which indicates that the soil is already capable of retaining water [4]. No runoff was observed in any of the rain events. Evapotranspiration ( $\frac{dET}{dt}$ ) was calculated because it affects the redistribution of soil moisture, which was obtained using the mass balance method (Equation (1)), remembering that evapotranspiration and rain cannot occur at the same time. The mass at instant  $i$  represents soil–water aggregates, and the mass of the vessel structure is considered zero as it was tared to zero before inserting the soil profile into the soil vessel.

#### 2.6. Validation

A total of 12 rain events of 2017 were analyzed from 8 February till 30 May, which were (i) February 13, (ii) 18 February, (iii) 19 February, (iv) 24 February, (v) 13 March, (vi) 14

March, (vii) 27 April, (viii) 28 April, (ix) 29 April, (x) 30 April, (xi) 10 May and (xii) 30 May. Approach 2 could be used only for events (v) to (x) while drainage occurred.

### 2.7. Model Calibrations

The results of the water infiltration rate  $\left(\frac{dI}{dt}\right)$  into the soil were used to calibrate empirical and physics infiltration models from the previously mentioned authors.

One of the most used models to represent the infiltration rate is the Kostiakov's model, which can be generally represented as Equation (8):

$$\frac{dI}{dt} = abt^{b-1} \quad (8)$$

where  $t$  is the infiltration time and  $a$  and  $b$  are empirical constants [4,6,46–48]. This equation has a boundary condition:  $\lim_{t \rightarrow \infty} \frac{dI}{dt} = 0$  [49,50]. All empirical parameters of all infiltration equations were determined by an iterative fit of the experimental data obtained with our approaches and selected using the best root mean square error (RMSE) in the fitting [46].

Parameter  $b$  of Kostiakov's equation is limited to being greater than zero and less than one. Therefore, the initial value of the infiltration rate tends to be infinite and has a basic rate to zero in an infinite time. In long irrigation events, Lewis [47] observed that the infiltration rate tends to a constant value before the end of the irrigation. So, in these long events, Kostiakov's equation usually overestimates the infiltration [51,52]. Therefore, a constant was added to this equation to represent the basic infiltration rate, which resulted in the modified Kostiakov's equation:

$$\frac{dI}{dt} = abt^{b-1} + c \quad (9)$$

where  $c$  is an empirical constant, which represents the basic infiltration rate [6,53,54]. This equation also is known as the Kostiakov–Lewis or Mezencev model. Its boundary condition is:  $\lim_{t \rightarrow \infty} \frac{dI}{dt} = \text{constant value} = c$  [49].

Philip's equation for the homogeneous porous medium infiltration rate is a simplification of Richard's model. The first term of the equation establishes the absorption of water into the soil and the second term represents a truncated series of small flooding times ( $A$ ), as the Equation (10):

$$\frac{dI}{dt} = \frac{1}{2}St^{-1/2} + A \quad (10)$$

where  $S$  is the sorptivity [50,53] and  $\lim_{t \rightarrow \infty} \frac{dI}{dt} = A$ , where  $A$  is a constant value [49].

Horton establishes an equation of infiltration capacity based on the behavior of nature that follows a law of inverse exponential. The infiltration rate decreases to a constant value, with an exponential decrease of change, and proportional to the infiltrated water volume as follows:

$$\frac{dI}{dt} = V_f + (V_0 - V_f)e^{-\beta \times t} \quad (11)$$

where  $V_f$  is the final infiltration rate or basic rate,  $V_0$  is the initial infiltration rate, and  $\beta$  is an empirical constant of change from the initial rate to the basic rate [17]. The boundary condition is  $\lim_{t \rightarrow \infty} \frac{dI}{dt} \geq 0$  [50].

When comparing the four models, it can be seen that the parameters of Kostiakov's model have no physical meaning and for longer times of water infiltration, it loses its representativeness and accuracy of the rate of water infiltration into the soil. For  $t = 0$ , the infiltration rate remains undetermined. In the modified Kostiakov's model, a term was added to represent the basic rate observed at long times of water infiltration. In the case of the Horton model, the initial infiltration rate is defined by a finite value and the model describes the behavior of the soil infiltration capacity curve. Finally, Philip described the rate of infiltration into the soil surface when there is a small amount of ponding, so its

terms do have physical significance for the behavior of the soil when water is allowed to enter.

The statistics used to evaluate the accuracy of the estimation of the water infiltration rate into the soil using the weighing lysimeter and using the above-mentioned models were: the standard deviation (s), the root mean square error (RMSE), and the coefficient of determination ( $R^2$ ) [55].

### 3. Results and Discussion

Figure 3 shows the mass curves of the two vessels of the lysimeter in the analyzed time interval. The initial data reported by the soil vessel indicates the mass of the soil particles plus the water content. Consequently, the mass variations reported after this initial point indicate the variations of the water content within the soil. In the curve of the soil vessel, the inputs were the rain and the irrigation and they can be differentiated by the type of increase they present. Irrigation has a very vertiginous increase in a short time, while the rain has a discontinuous growth in time, on the other hand, the descents can represent the evapotranspiration losses, drainage losses or both.

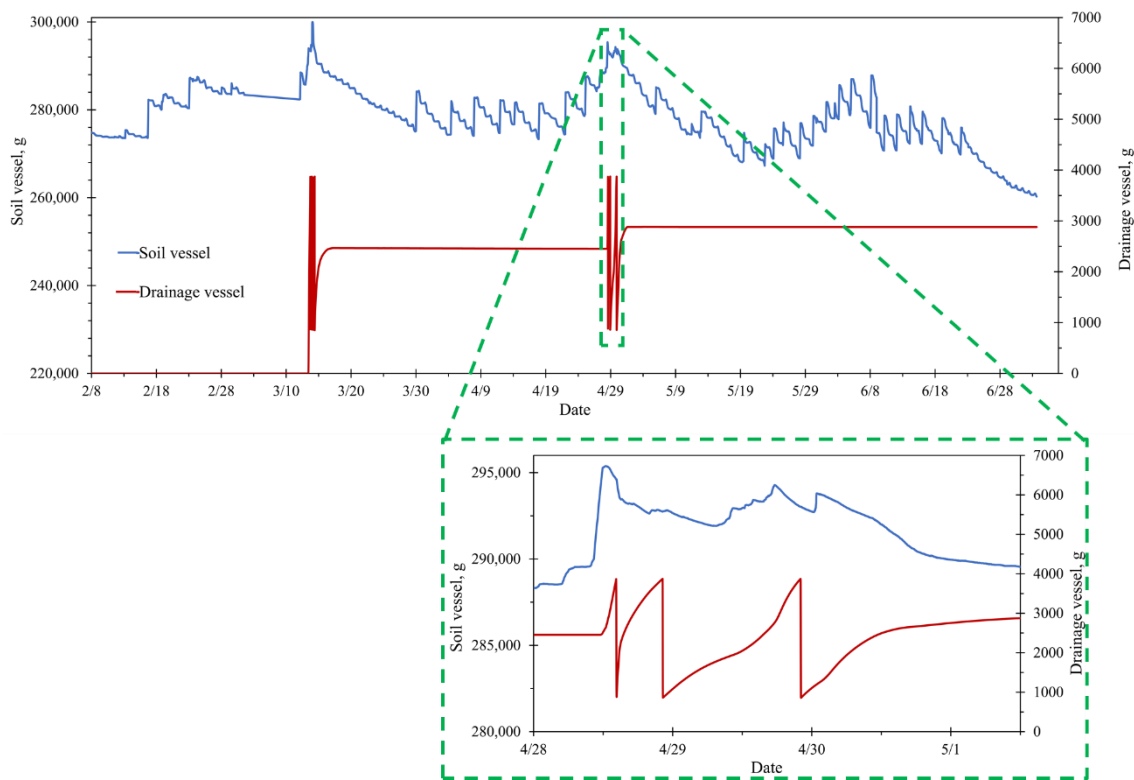


**Figure 3.** Mass variations of the two lysimeter vessels during 2017.

In the case of the data from the drainage vessel (red curve), the rise of the curve represents that the drainage has started and the sudden descents show us the emptying of the vessel. As shown in the Figure 3, only two drainage events were registered by the vessel on 13–14 March and 28–30 April. The drainage vessel was programmed to open its valve at 3000 g of storage and discharge (to avoid damaging the load cell). Therefore, the drainage vessel curve in the Figure 3 shows accumulated masses less than 4000 g. The emptying is almost instantaneous, it takes less than 3 min and, as mentioned, no drop is lost. The March event caused more drainage than the April event, in less time of rain. This indicates that the rain intensity of the March event was higher than in the April event, as more water fell in less time. The seven rainfall events between February and March contributed to the first drainage event occurred in 14 March. Meanwhile, the five rainfall events occurred between April and May caused the second drainage event in 28–30 April.

### 3.1. Estimation of Rain Inflow

The rainy days total of 12 were analyzed and were determined with the Equation (4), representing 12 events. The Table 1 shows the rainfall recorded by day in the weighing lysimeter and those observed in a rain gauge installed near the weighing lysimeter at 800 m. The rain calculated with the lysimeter for the first analysis day concerning the Instituto Técnico Agronómico Provincial (ITAP, Spanish acronym) station has a difference of 0.05 mm. The differences found can be explained by the space behavior of the rainfall variability in a region, which has a greater impact in semi-arid zones such as the study zone [56]. There is an absolute average difference of 1.59 mm between the two devices.

**Table 1.** Rainfall intensity data of the analyzed days recorded by two different devices.

Date	Rain Registered per Day	
	Weighing Lysimeter	Weather Station ITAP
	(mm)	(mm)
02/13	3.55	3.60
02/18	3.16	3.30
02/19	2.76	2.90
02/24	1.30	1.00
03/13	36.77	26.70
03/14	28.53	22.30
04/27	7.04	6.40
04/28	7.06	5.90
04/29	8.16	8.30
04/30	2.44	1.6
05/10	1.01	1.10
05/30	2.11	1.60

### 3.2. Estimation of Soil Moisture Content

The soil moisture content was obtained using the gravimetric method (Equation (7)). Two drainage events were caused with the rain events of 13–14 March, 28–30 April so only with these events was possible to determine the soil field capacity ( $\theta_{FC}$ ) based on its definition. The Figure 4 shows the rain behavior and its relation to the moisture content of the soil, which shows that when rain is falling, there is a mass increase, and when the soil reaches the field capacity and the rain continues, there is drainage; when there is a fall in the humidity curve, drainage increases.

By plotting the water content curve with that of the drainage vessel (red curve) it was possible to determine the moment when the moisture content at field capacity of the soil ( $\theta_{FC}$ ) was reached. In both months, the  $\theta_{FC}$  was established when the drainage vessel curve became constant, indicating that the soil had stopped draining and there was no variation in the weighing lysimeter.

A horizontal line was drawn on the water content at the instant the mass drainage vessel was not increased, indicating that the  $\theta_{FC}$  was reached and was established two days after the beginning of the rain in  $0.33 \text{ cm}^3/\text{cm}^3$ .

Since the  $\theta_{FC}$  was established days after the rain events, evapotranspiration ( $\frac{dET}{dt}$ ) was presents, so it was calculated as indicated by [27,32,43] in their work. Table 2 has the water balance of the days involved in the calculation of the  $\theta_{FC}$ .  $\frac{dET}{dt}$  is a variable that subtracts moisture from the soil surface, this variable for the first days of each event only represents 0% of water losses and rainfall; it increases as the rain decreases over the days, so that in the second day  $\frac{dET}{dt}$  represents 15.47% and 10.32% of water losses and 18.96% and 7.83% of rainfall. The total  $\frac{dET}{dt}$  losses for all days of each event used for the  $\theta_{FC}$  calculation represent 11.04% for the first (Figure 4a) and 24.37% for the second (Figure 4b).  $\frac{dET}{dt}$  represents 8.28% of the rain of the first event (Figure 4a) and 35.38% of the second event (Figure 4b).



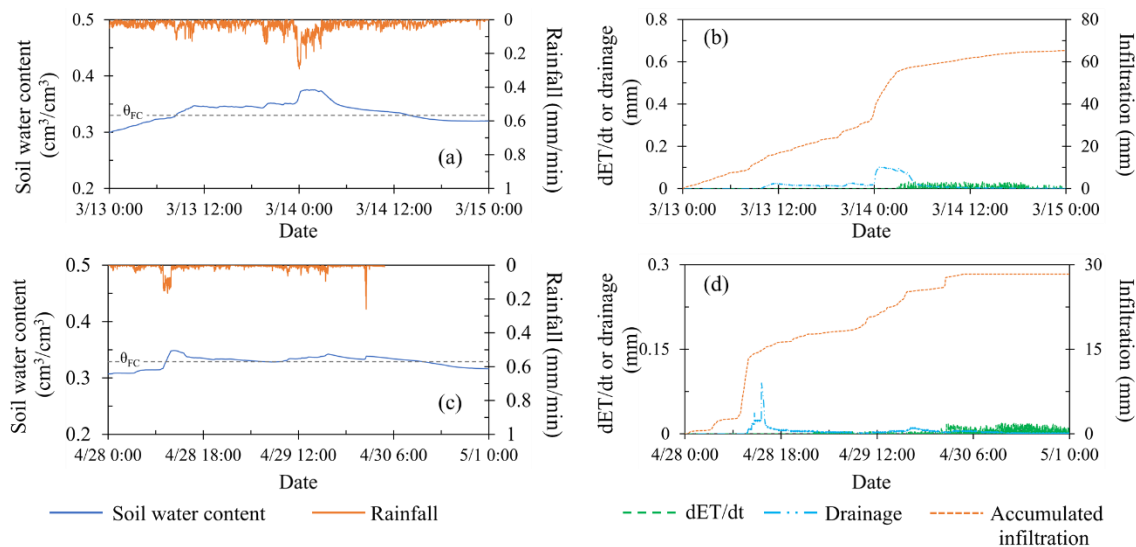


**Figure 4.** Soil water content and hydrologic variables obtained with the weighing lysimeter, (a) Soil water content and rainfall of March; (b) evapotranspiration ( $\frac{dET}{dt}$ ) and infiltration of March; (c) soil water content and rainfall of April; (d)  $\frac{dET}{dt}$  and infiltration of April.

**Table 2.** Water balance of the days involved in determining the  $\theta_{FC}$ .

Date	$\frac{dIR}{dt}$ , mm	$\frac{dP}{dt}$ , mm	$\frac{dD}{dt}$ , mm	$\frac{dET}{dt}$ , mm
03/13	0.00	36.77	14.04	0.00
03/14	0.00	28.53	29.57	5.41
04/28	10.62	5.90	8.65	0.00
04/29	0.00	8.30	5.65	0.65
04/30	0.00	1.60	3.05	4.94

The Table 3 reports the moisture content at field capacity values obtained and some that report the literature for a silty loam soil. The values with less standard deviation with the result of the weighing lysimeter were the value obtained in the laboratory in this investigation and the maximum value reported by Assi et al. [57] with 0.014 cm<sup>3</sup>/cm<sup>3</sup>. These are followed by the values reported by FAO [58] in graphs and tables based on soil texture to obtain the hydrodynamic characteristics of the soil ( $\theta_{saturation}$ ,  $\theta_{FC}$  and  $\theta_{wilting\ point}$ ) with 0.02 cm<sup>3</sup>/cm<sup>3</sup>, which shows a good agreement with results obtained in laboratory and lysimeter.

**Table 3.** Comparison of field water content value obtained in the soil with literature values.

$\theta_{FC}$ , cm <sup>3</sup> /cm <sup>3</sup>	Method of Estimation and Authors
0.33	Weighing Lysimeter
0.35	Laboratory
0.22–0.36	FAO [58]
0.30–0.31	Pedostucture [57]
0.244	Gravimetric [59]

### 3.3. Water Infiltration Rate

Seven rains were analyzed with the Approach 1. The soil was below field capacity so that the positive variations reported soil vessel indicated the water infiltration rate (13, 18, 19 and 24 February, 27 April and 10 and 30 May). According to USDA [60] and Evanylo and McGuinn [61] the best way to determine the rate or speed of infiltration is when the soil is close to field capacity; four rain events had drainage due to soil was above field capacity; in these rains, approach 2 was applied (13–14 March and 28, 29 and 30 April).

Figure 5 shows the 11 scatter soil water infiltration rate diagrams of the rain 12 events analyzed, most of the graphs have a duration of less than 24 h. The soil shows a very similar behavior in all the graphs, it starts with lower rates until it reached a maximum peak and then decreases to a stable or basic rate. The basic infiltration rate was obtained considering the eleven rainfall events in 1.49 mm/h with a 0.36 mm/h standard deviation. According to USDA [60], this rate occurs when the soil is almost saturated and it does not decrease or increase as more water is added.

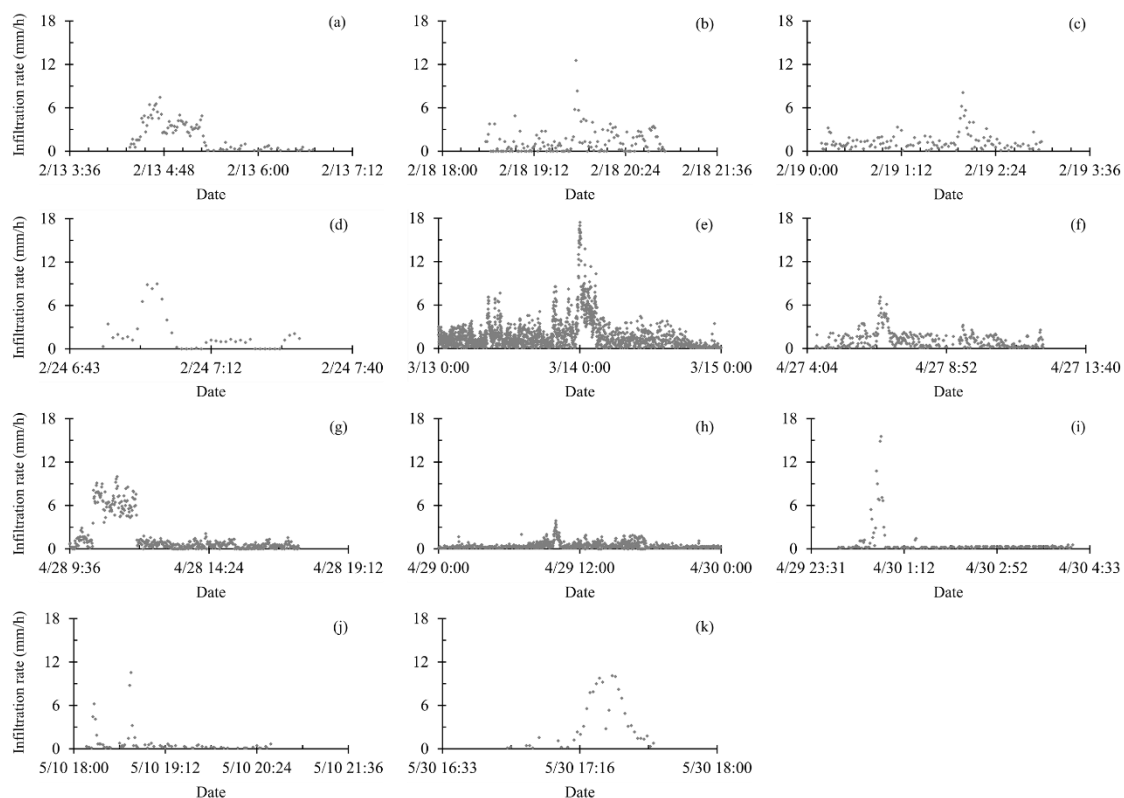


**Figure 5.** Soil water infiltration rate scatter diagrams, (a) 13 February; (b) 18 February; (c) 19 February; (d) 24 February; (e) 13–14 March; (f) 27 April; (g) 28 April; (h) 29 April; (i) 30 April; (j) 10 May; (k) 30 May.

The variability of the standard deviation could be due the experimental error. The infiltration rate or speed modifications reaching a 23%, could probably be due the flow paths alterations at forcing the water to pass through an orifice. Further research is needed in order to minimize this variability, i.e., a number of orifices placed in the horizontal plane in the soil vessel bottom could represent a variability of the measured infiltration rate/speed minimizing the measurement errors. Nevertheless, our methodology represents an approach to estimate the infiltration rate and could be compared with other methodologies.

The variability of the initial infiltration rate may be due to rainfall intensity and initial moisture content [62,63]. The initial moisture contents of the seven infiltration rate scatter diagrams below field capacity ranged from 0.23 to 0.30  $\text{cm}^3/\text{cm}^3$  and the other four scatter diagrams were 0.30 to 0.33  $\text{cm}^3/\text{cm}^3$ .

The basic infiltration found in both approaches (summarized in the Table 4) were low compared to the values reported in the literature. However, the values found in this investigation coincide with those reported by Li et al. [64] for homogeneous wetting and their value was obtained with an initial soil water content of 0.034  $\text{m}^3/\text{m}^3$ , which was air-dried and placed in a 50 cm column. The lower value obtained in Li et al. [64] was with a slightly water-repellent silty loam soil (this is achieved by adding octadecylamine to the soil).

**Table 4.** Values of the infiltration rate of a silty loam soil.

Basic Infiltration Rate, mm/h	Method and Authors
1.13–1.85	Weighing lysimeter
10.00–14.00	Concentric cylinders [65]
2.00–3.00	Homogeneous wetting [64]
0.15–0.30	Slightly water-repellent soil [64]
5.00–8.00	Concentric cylinders [6]

The basic infiltration rate obtained with the weighing lysimeter, was lower compared with the research works of Maldonado [65] and Ali [6] considering the same soil type. Some factors that could have caused the low value of the basic infiltration rate are organic matter content, vegetative cover, and the crop root [6,63]. Nevertheless, further investigation is needed to corroborate it.

The results obtained with the two proposed approaches are simple and representative of the current capacity of infiltration of the soil, where roots have been growing within the soil profile, fertilizers have been added, and the profile has been compacted by the same force exerted by rainwater and irrigation. All of this is not reflected in the values seen in Table 4.

### 3.4. Model Calibrations

The 11 infiltration curves were calibrated with the four models described above, from its highest point. In Figure 6, only the four models with longer rainfall duration are presented. The model that showed the best fit was Horton's, with a RMSE of  $0.89 \pm 0.40$  and  $R^2$  of  $0.65 \pm 0.30$ , followed by Kostiakov with a RMSE of  $1.06 \pm 0.40$  and  $R^2$  of  $0.63 \pm 0.23$ , modified Kostiakov with a RMSE of  $1.03 \pm 0.43$  and  $R^2$  of  $0.62 \pm 0.22$ , and Philip with a RMSE of  $1.30 \pm 0.42$  and  $R^2$  of  $0.48 \pm 0.17$ . The only model that established a lower initial infiltration rate was Horton.

The models establish the value for the basic infiltration rate in some of its variables in the equation. In the case of Kostiakov, it does not have an established value. Modified Kostiakov established the basic infiltration at  $0.14 \pm 0.14$  mm/h (in its constant  $c$ ) [53,54], Philip at  $0.16 \pm 0.11$  mm/h (in  $A$ ), and Horton at  $0.38 \pm 0.34$  mm/h (in  $V_f$ ) [17,50]. The models calibration showed a behavior as indicated by their boundary limits, as the infiltration rate tends to constant values close to zero when time tends to infinity [49,50].

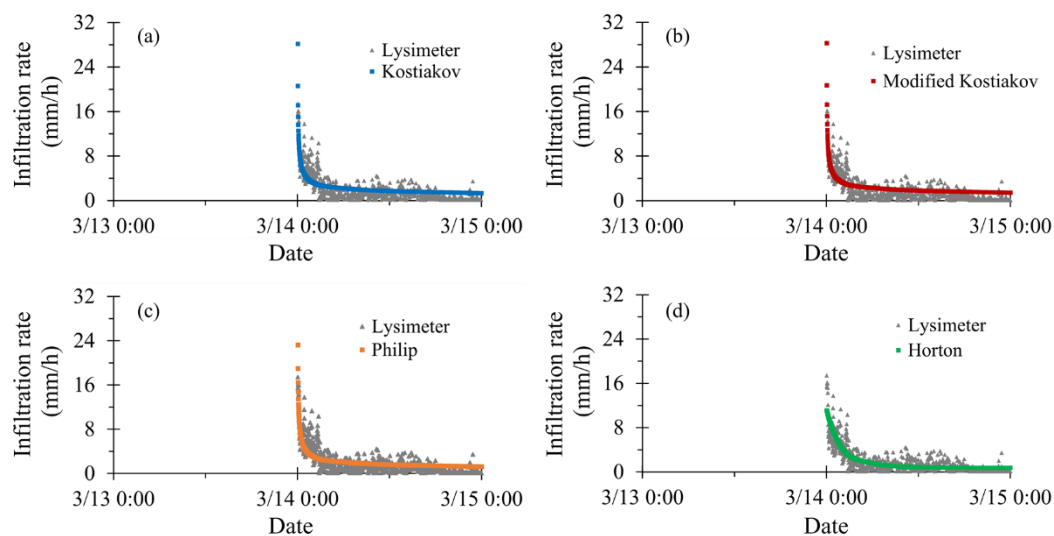


**Figure 6.** Adjustment of the infiltration models to the values of March 13–14, (a) Kostiakov model; (b) Modified Kostiakov model; (c) Philip model; (d) Horton model.

In the research works of Rodríguez-Vásquez et al., [66] and Mirzaee et al., [67] measured infiltration rate with double ring infiltrometer apparatus for silt loam and clayey soil, their parameter values obtained for the different infiltration models are shown in the Table 5. In the first work, the water contents were between 24.3% and 31.1%, while in the second article this was not mentioned, and our range was of 0.23–0.33 cm<sup>3</sup>/cm<sup>3</sup>.

**Table 5.** Parameters values of infiltration models for silt loam soil.

Model		Lysimeter	Rodríguez-Vásquez et al. [66]	Mirzaee et al. [67]
Kostiakov	a	47.70	66.46	1.00
	b	0.62	1.12	3.11
Modified Kostiakov	a	48.42		3.23
	b	0.50	-	0.84
	c	0.29		1.00
Philip	S	20.83	13.6	31.3
	A	0.30	7.93	1.00
Horton	$V_O$	14.44		58.8
	$V_f$	0.75	-	34.8
	$\beta$	0.28		1.00

The fit parameters of Kostiakov model in this investigation compared with the Rodríguez-Vásquez et al., [66], have a difference of 39% for the parameter a, while for the parameter b is of 20%. In the Philip model, there is a difference of 35% for S parameter and the value of A parameter of Rodríguez-Vásquez et al., [66] is 25 times higher than ours. This difference probably is due to that error of estimation is greater in the concentric cylinders.

There is a significant difference with respect to Mirzaee et al., [67] work in the four models varying from 68 to 245%. because their reported values are of a soil profile with silty-loam and clayey horizons, which the infiltration capacity is very low due to characteristics of the clays.

#### 4. Conclusions

In this research, the mass values of a compact weighing lysimeter were used to measure soil moisture behavior and the water infiltration rate of a soil silt loam under unsteady rainfall conditions, using two approaches, the first part when the soil is below and the second when the soil is above field capacity. The results showed that with the two approaches it is possible to establish the soil infiltration curve and for short and long application times in real conditions. The soil is subject to a variable and faster infiltration rate at the beginning, but it reaches a basic or stable infiltration as the soil fills its pores.

These approaches are simple but satisfy the conservation of mass and continuity equation for incompressible flows. Although they are used for non-saturation conditions, they can be used for saturation conditions by adding the surface runoff variable that would subtract incoming flow to the soil.

The use of the weighing lysimeter with these approaches allowed to characterize the infiltration rate of a homogeneous and non-homogeneous soil at depths where agriculture regularly takes place. However, the limitation is that it is not possible to monitor the progress of the wet front, so further research is necessary in order to have greater measurement instruments (i.e., soil moisture sensors) to characterize the water movement in the soil and the forces acting within it (i.e., soil water potential sensor).

**Author Contributions:** Conceptualization and methodology, L.Á.-D.; experiment development J.M.M.-M. and M.S.-M.; data analysis, L.Á.-D., J.M.M.-M., and M.S.-M.; calibration and fitting of the mathematical models, C.F.B.-C., J.G.-T., and H.E.J.-F.; investigation, L.Á.-D., C.F.B.-C., J.G.-T., C.O.R.R., and J.M.M.-M.; writing—original draft preparation, L.Á.-D.; writing—review and editing, C.F.B.-C., J.G.-T., H.E.J.-F., and C.O.R.R.; funding acquisition M.S.-M. and J.M.M.-M. All authors have read and agreed to the published version of the manuscript.

**Funding:** Project of Research and Development with reference IDI-20190146 titled “Development and implementation of a ferticontrol equipment by weighing lysimetry for use in intensive agriculture”, in collaboration with the AGROSOLMEN, S.L. company, co-financed by the European Regional Development Fund (FEDER) through the Spanish Pluri-regional Operational Programme 2014–2020.

**Institutional Review Board Statement:** Not applicable.

**Informed Consent Statement:** Not applicable.

**Data Availability Statement:** No new data were created or analyzed in this study. Data sharing is not applicable to this article.

**Acknowledgments:** The authors express their gratitude to the Mexican National Council for Science and Technology (CONACYT) for financing the scholarship of the doctoral student.

**Conflicts of Interest:** The authors declare no conflict of interest. The funders had no role in the design of the study; in the collection, analyses, or interpretation of data; in the writing of the manuscript, or in the decision to publish the results.

## References

1. Struthers, I.; Hinz, C.; Sivapalan, M.; Deutschmann, G.; Beese, F.; Meissner, R. Modelling the water balance of a free-draining lysimeter using the downward approach. *Hydrol. Process.* **2003**, *17*, 2151–2169. [[CrossRef](#)]
2. Wegehenkel, M.; Zhang, Y.; Zenker, T.; Diestel, H.; Zhang, Y. The use of lysimeter data for the test of two soil-water balance models: A case study. *J. Plant Nutr. Soil Sci.* **2008**, *171*, 762–776. [[CrossRef](#)]
3. Feltrin, R.M.; de Paiva, J.B.D.; de Paiva, E.M.C.D.; Beling, F.A. Lysimeter soil water balance evaluation for an experiment developed in the Southern Brazilian Atlantic Forest region. *Hydrol. Process.* **2011**, *25*, 2321–2328. [[CrossRef](#)]
4. Kirkham, M. Water Movement in Saturated Soil. *Princ. Soil Plant. Water Relat.* **2014**, *87*–101. [[CrossRef](#)]
5. Mendes, W.R.; de Araújo, F.M.U.; Dutta, R.; Heeren, D.M. Fuzzy control system for variable rate irrigation using remote sensing. *Expert Syst. Appl.* **2019**, *124*, 13–24. [[CrossRef](#)]
6. Ali, M.H. *Fundamentals of Irrigation and On-farm Water Management: Volume 1*; Springer Science and Business Media LLC: Berlin/Heidelberg, Germany, 2010.
7. Herrada, M.A.; Gutiérrez-Martin, A.; Montanero, J.M. Modeling infiltration rates in a saturated/unsaturated soil under the free draining condition. *J. Hydrol.* **2014**, *515*, 10–15. [[CrossRef](#)]
8. Mattar, M.A.; Alazba, A.A.; El-Abedin, T.K. Forecasting furrow irrigation infiltration using artificial neural networks. *Agric. Water Manag.* **2015**, *148*, 63–71. [[CrossRef](#)]
9. Yuan, J.; Feng, W.; Jang, X.; Wang, J. Saline-alkali migration in soda saline soil based on sub-soiling technology. *Desalin. Water Treat.* **2019**, *149*, 352–362. [[CrossRef](#)]
10. Duchaufour, P. *Manual de Edafología*; Masson S.A.: Barcelona, Spain, 1987; ISBN 9788431104191.
11. Plaster, E.J. *Soil Science & Management*; Editorial Paraninfo: Madrid, Spain, 2000; ISBN 84-283-2643-6.
12. Wang, K.; Yang, X.; Liu, X.; Liu, C. A simple analytical infiltration model for short-duration rainfall. *J. Hydrol.* **2017**, *555*, 141–154. [[CrossRef](#)]
13. Villalobos, F.J.; Mateos, L.; Orgaz, F.; Fereres, E. *Fitotecnia Bases y Tecnologías de La Producción Agrícola*; Mundi-Pren: Madrid, Spain, 2002; ISBN 9788484760498.
14. Martín-Benito, J.M. *El Riego Por Aspersión*; Universidad de Castilla La Mancha: Ciudad Real, Spain, 1991.
15. Harper, R.; McKissock, I.; Gilkes, R.; Carter, D.; Blackwell, P. A multivariate framework for interpreting the effects of soil properties, soil management and landuse on water repellency. *J. Hydrol.* **2000**, *232*, 371–383. [[CrossRef](#)]
16. Richards, L.A. Capillary Conduction of Liquids Through Porous Mediumus. *Physics* **1931**, *1*, 318–333. [[CrossRef](#)]
17. Horton, R.E. An Approach Toward a Physical Interpretation of Infiltration—Capacity 1. *Soil Sci. Soc. Am. J.* **1941**, *5*, 399–417. [[CrossRef](#)]
18. Mahmood, S.; Latif, M. A Simple Procedure for Simulating Surge Infiltration Using First-Surge Infiltrometer Data. *Irrig. Drain.* **2005**, *54*, 407–416. [[CrossRef](#)]
19. Teófilo-Salvador, E.; Morales-Reyes, G.P. Propuesta del modelo físico del infiltrómetro de cilindros concéntricos rediseñado multifuncional (ICCRM). *Tecnol. Cienc. Agua* **2018**, *9*, 103–131. [[CrossRef](#)]
20. Arriaga, F.J.; Kornecki, T.S.; Balkcom, K.S.; Raper, R.L. A method for automating data collection from a double-ring infiltrometer under falling head conditions. *Soil Use Manag.* **2009**, *26*, 61–67. [[CrossRef](#)]
21. Fatehnia, M.; Paran, S.; Kish, S.; Tawfiq, K. Automating double ring infiltrometer with an Arduino microcontroller. *Geoderma* **2016**, *262*, 133–139. [[CrossRef](#)]
22. Groh, J.; Vanderborght, J.; Pütz, T.; Vereecken, H. How to Control the Lysimeter Bottom Boundary to Investigate the Effect of Climate Change on Soil Processes? *Vadose Zone J.* **2016**, *15*, 1–15. [[CrossRef](#)]
23. Lepore, B.J.; Norman, J.M.; Lowery, B.; Brye, K.R. Soil Compaction above Long-Term Lysimeter Installations. *Soil Sci. Soc. Am. J.* **2011**, *75*, 30–34. [[CrossRef](#)]

24. Masarik, K.C.; Norman, J.M.; Mason, R.E.; Baker, J.M. Improvements to Measuring Water Flux in the Vadose Zone. *J. Environ. Qual.* **2004**, *33*, 1152–1158. [[CrossRef](#)]
25. Jiménez-Buendía, M.; Ruiz-Peñalver, L.; Vera-Repullo, J.; Intrigliolo-Molina, D.; Molina-Martínez, J. Development and assessment of a network of water meters and rain gauges for determining the water balance. New SCADA monitoring software. *Agric. Water Manag.* **2015**, *151*, 93–102. [[CrossRef](#)]
26. Ruiz-Peñalver, L.; Vera-Repullo, J.; Jiménez-Buendía, M.; Guzman, I.; Molina-Martínez, J. Development of an innovative low cost weighing lysimeter for potted plants: Application in lysimetric stations. *Agric. Water Manag.* **2015**, *151*, 103–113. [[CrossRef](#)]
27. Haselow, L.; Meissner, R.; Rupp, H.; Miegel, K. Evaluation of precipitation measurements methods under field conditions during a summer season: A comparison of the standard rain gauge with a weighable lysimeter and a piezoelectric precipitation sensor. *J. Hydrol.* **2019**, *575*, 537–543. [[CrossRef](#)]
28. Meissner, R.; Seeger, J.; Rupp, H.; Seyfarth, M.; Borg, H. Measurement of dew, fog, and rime with a high-precision gravitation lysimeter. *J. Plant. Nutr. Soil Sci.* **2007**, *170*, 335–344. [[CrossRef](#)]
29. Schrader, F.; Durner, W.; Fank, J.; Gebler, S.; Pütz, T.; Hannes, M.; Wollschläger, U. Estimating Precipitation and Actual Evapotranspiration from Precision Lysimeter Measurements. *Procedia Env. Sci.* **2013**, *19*, 543–552. [[CrossRef](#)]
30. Valtanen, M.; Sillanpää, N.; Setälä, H. A large-scale lysimeter study of stormwater biofiltration under cold climatic conditions. *Ecol. Eng.* **2017**, *100*, 89–98. [[CrossRef](#)]
31. Marek, G.; Gowda, P.; Marek, T.; Auvermann, B.; Evett, S.; Colaizzi, P.; Brauer, D. Estimating pre-season irrigation losses by characterizing evaporation of effective precipitation under bare soil conditions using large weighing lysimeters. *Agric. Water Manag.* **2016**, *169*, 115–128. [[CrossRef](#)]
32. Hannes, M.; Wollschläger, U.; Schrader, F.; Durner, W.; Gebler, S.; Pütz, T.; Fank, J.; Von Unold, G.; Vogel, H.-J. High-resolution estimation of the water balance components from high-precision lysimeters. *Hydrol. Earth Syst. Sci. Discuss.* **2015**, *12*, 569–608. [[CrossRef](#)]
33. López-Urrea, R.; Montoro, A.; Mañas, F.; López-Fuster, P.; Fereres, E. Evapotranspiration and crop coefficients from lysimeter measurements of mature ‘Tempranillo’ wine grapes. *Agric. Water Manag.* **2012**, *112*, 13–20. [[CrossRef](#)]
34. Luo, Y.; Sophocleous, M. Seasonal groundwater contribution to crop-water use assessed with lysimeter observations and model simulations. *J. Hydrol.* **2010**, *389*, 325–335. [[CrossRef](#)]
35. Kelleners, T.J.; Soppe, R.; Ayars, J.E.; Šimunek, J.; Skaggs, T.H. Inverse Analysis of Upward Water Flow in a Groundwater Table Lysimeter. *Vadose Zone J.* **2005**, *4*, 558–572. [[CrossRef](#)]
36. Dijkema, J.; Koonce, J.; Shillito, R.; Ghezzehei, T.; Berli, M.; van der Ploeg, M.; Van Genuchten, M. Water Distribution in an Arid Zone Soil: Numerical Analysis of Data from a Large Weighing Lysimeter. *Vadose Zone J.* **2017**, *17*, 170035. [[CrossRef](#)]
37. Germann, P.; Prasuhn, V. Viscous Flow Approach to Rapid Infiltration and Drainage in a Weighing Lysimeter. *Vadose Zone J.* **2017**, *17*, 170020. [[CrossRef](#)]
38. Schwaerzel, K.; Bohl, H.P. An easily installable groundwater lysimeter to determine water balance components and hydraulic properties of peat soils. *Hydrol. Earth Syst. Sci.* **2003**, *7*, 23–32. [[CrossRef](#)]
39. Google Earth. Available online: <https://earth.google.com/web/> (accessed on 14 March 2020).
40. Conklin, H.E. Soil Survey Manual. *J. Farm. Econ.* **1952**, *34*, 145. [[CrossRef](#)]
41. Automatic Weather Station Network. Criteria for the Localization of Sites and Installation of Sensor. Acquisition Characteristics and Sampling. In *UNE 500520-2002*; Spanish Standardization (UNE, Spanish Acronyms). Elaborated by the Technical Committee AEN/CTN GET5 Meteorological Records Whose Secretariat Is Provided by AENOR-PUERTOS DEL ESTADO; Spanish Association for Standardization and Certification (AENOR, Spanish Acronyms): Madrid, Spain, 2002.
42. Nicolás-Cuevas, J.A.; Parras-Burgos, D.; Soler-Méndez, M.; Ruiz-Canales, A.; Molina-Martínez, J.M. Removable Weighing Lysimeter for Use in Horticultural Crops. *Appl. Sci.* **2020**, *10*, 4865. [[CrossRef](#)]
43. Peters, A.; Nehls, T.; Schonsky, H.; Wessolek, G. Separating precipitation and evapotranspiration from noise—A new filter routine for high-resolution lysimeter data. *Hydrol. Earth Syst. Sci.* **2014**, *18*, 1189–1198. [[CrossRef](#)]
44. Gebler, S.; Hendricks-Franssen, H.-J.; Putz, T.; Post, H.; Schmidt, M.; Vereecken, H. Actual evapotranspiration and precipitation measured by lysimeters: A comparison with eddy covariance and tipping bucket. *Hydrol. Earth Syst. Sci.* **2015**, *19*, 2145–2161. [[CrossRef](#)]
45. Wang, N.; Chu, X. Revised Horton model for event and continuous simulations of infiltration. *J. Hydrol.* **2020**, *589*, 125215. [[CrossRef](#)]
46. Hartley, D.M. Interpretation of Kostiakov Infiltration Parameters for Borders. *J. Irrig. Drain. Eng.* **1992**, *118*, 156–165. [[CrossRef](#)]
47. Lewis, M.R. The rate of infiltration of water in irrigation-practice. *Trans. Am. Geophys. Union* **1937**, *18*, 361–368. [[CrossRef](#)]
48. Fok, Y. Derivation of Lewis-Kostiakov Intake Equation. *J. Irrig. Drain. Eng.* **1986**, *112*, 164–171. [[CrossRef](#)]
49. Haverkamp, R.; Kutilek, M.; Parlange, J.Y.; Rendon, L.; Krejca, M. Infiltration under Ponded Conditions: 2. Infiltration Equations Tested for Parameters Time-Dependence and Predictive Use1. *Soil Sci.* **1988**, *145*, 317–329. [[CrossRef](#)]
50. Philip, J.R. The Theory of Infiltration: 4. Sorptivity and Algebraic Infiltration Equation. *Soil Sci.* **1957**, *84*, 257–264. [[CrossRef](#)]
51. Smerdon, E.T.; Blair, A.W.; Reddell, D.L. Infiltration from Irrigation Advance Data. I: Theory. *J. Irrig. Drain. Eng.* **1988**, *114*, 4–17. [[CrossRef](#)]
52. Haghbi, A.H.; Abedi-Koupai, J.; Heidarpour, M.; Mohammadzadeh-Habili, J. A New Method for Estimating the Parameters of Kostikov and Modified Kostiakov Infiltration Equations. *World Appl. Sci. J.* **2011**, *15*, 129–135.

53. Strelkoff, T.S.; Clemmens, A.J.; Bautista, E. Field Properties in Surface Irrigation Management and Design. *J. Irrig. Drain. Eng.* **2009**, *135*, 525–536. [[CrossRef](#)]
54. Furman, A.; Warrick, A.W.; Zerihun, D.; Sanchez, C.A. Modified Kostiakov Infiltration Function: Accounting for Initial and Boundary Conditions. *J. Irrig. Drain. Eng.* **2006**, *132*, 587–596. [[CrossRef](#)]
55. Wackerly, D.D.; Mendenhall, W.; Schaeffer, R.L. *Mathematical Statics with Applications*, 7th ed.; Cengage Learning: Boston, MA, USA, 2010.
56. Belmonte, A.M.C.; García, J.S.; García, M.J.L. The effect of observation timescales on the characterisation of extreme Mediterranean precipitation. *Adv. Geosci.* **2010**, *26*, 61–64. [[CrossRef](#)]
57. Assi, A.; Blake, J.; Mohtar, R.H.; Braudeau, E. Soil aggregates structure-based approach for quantifying the field capacity, permanent wilting point and available water capacity. *Irrig. Sci.* **2019**, *37*, 511–522. [[CrossRef](#)]
58. Allen, R.G.; Pereira, L.S.; Raes, D.; Smith, M. *Crop Evapotranspiration-Guidelines for Computing Crop Water Requirements*; FAO Irrigation and Drainage Paper 56; FAO Rome: Roma, Italy, 1998; Volume 300, p. d05109.
59. Porta-Casanellas, J.; Lopez-Acevedo, R.M. *Agenda de Campo de Suelos. Información de Suelos Para La Agricultura y El Medio Ambiente*; Ediciones Mundi-Prensa: Madrid, Spain, 2005.
60. USDA (United State Department of Agricultura); NRCS (Natural Resources Conservation Service); ARS (Agricultural Research Service); SQI (Soil Quality Institute). *Soil Quality Test Kit Guide*; U.S. Department of Agriculture: Washington, DC, USA, 2001.
61. Evanylo, G.; McGuinn, R. *Agricultural Management Practices and Soil Quality*; Virginia Polytechnic Institute and State University, College of Agriculture and Life Sciences: Blacksburg, VA, USA, 2000; Volume 5.
62. Cui, Z.; Wu, G.-L.; Huang, Z.; Liu, Y. Fine roots determine soil infiltration potential than soil water content in semi-arid grassland soils. *J. Hydrol.* **2019**, *578*, 124023. [[CrossRef](#)]
63. Liu, Y.; Cui, Z.; Huang, Z.; López-Vicente, M.; Wu, G.-L. Influence of soil moisture and plant roots on the soil infiltration capacity at different stages in arid grasslands of China. *Catena* **2019**, *182*, 104147. [[CrossRef](#)]
64. Li, Y.; Ren, X.; Hill, R.; Malone, R.; Zhao, Y.; Ying, Z.; Malonew, R. Characteristics of Water Infiltration in Layered Water-Repellent Soils. *Pedosphere* **2018**, *28*, 775–792. [[CrossRef](#)]
65. Maldonado, T. Manual de Riego Parcelario. Available online: [http://www.fao.org/tempref/GI/Reserved/FTP\\_FaoRlc/old/prior/recnat/pdf/MR\\_cap1.PDF](http://www.fao.org/tempref/GI/Reserved/FTP_FaoRlc/old/prior/recnat/pdf/MR_cap1.PDF) (accessed on 30 January 2020).
66. Rodríguez-Vásquez, A.F.; Aristizábal-Castillo, A.M.; Camacho-Tamayo, J.H. Variabilidad Espacial de los Modelos de Infiltración de Philip y Kostiakov en un Suelo Ándico. *Eng. Agríc.* **2008**, *12*, 64–75. [[CrossRef](#)]
67. Mirzaee, S.; Zolfaghari, A.A.; Gorji, M.; Dyck, M.; Dashtaki, S.G. Evaluation of infiltration models with different numbers of fitting parameters in different soil texture classes. *Arch. Agron. Soil Sci.* **2013**, *60*, 681–693. [[CrossRef](#)]